Application of a Particle Image Velocimetry (PIV) System to the Periodic Unsteady Flow Around an Isolated Compressor Blade

A. Lehr, A. Bölcs
Swiss Federal Institute of Technology
Lausanne, Switzerland

ABSTRACT
Today, Particle Image Velocimetry (PIV) is often used to investigate time dependant flows because of its ability to deliver instantaneous flow field information across an illuminated plane with high spatial and temporal resolution. In the present paper the application of this measurement technique to the transonic flow around an isolated compressor blade in a Laval nozzle is presented. The PIV technique is not only able to deliver instantaneous flow field information, but also yields the mean velocity field and turbulence quantities of the flow by statistical treatment of the instantaneous data sets.

For the first test series, the PIV system was used to measure the steady flow field around the compressor blade. In another test series, measurements of the time dependant periodic flow field were conducted by means of PIV. These results quantify the unsteady motion of the normal shock on the suction side of the blade. Finally, phase averaging of the instantaneous flow quantities yields a large database for statistical treatment (e.g. turbulence) and the ability to compare the averaged results with traditional measurement techniques.

NOMENCLATURE

c	[m]	Chord length of the blade
d	[mm]	diameter
f	[mm]	Focal length
f	[Hz]	Excitation frequency
F-number	[-]	Relative aperture of the camera lens
i	[°]	Incidence angle
k	[-]	Reduced frequency, $f\pi c/U_1$
M	[-]	Mach number
n	[-]	Fit power for averaging
N	[-]	Number of (picture/vector) samples
r	[mm]	Fit radius for averaging
Re	[-]	Reynolds number based on chord length, $U_1 c/\nu_1$
T	[K]	Temperature
(u,v,w)	[m/s]	Mean velocity vector
x	[mm]	Cartesian coordinate in axial direction
y	[mm]	Cartesian coordinate in cross duct direction
z	[mm]	Cartesian coordinate in span direction
φ	[°]	Phase angle of the rotating blade (gust generator)
μ	[kg/ms]	Dynamic viscosity
ρ	[kg/m^3]	Density
ν	[m^2/s]	Kinematic viscosity
τ_S	[s]	Relaxation time $\tau_S = d_P^2 \rho_P / (18\mu)$
Φ	[°]	Phase angle between excitation source and aerodynamic response

Subscripts

$1, \infty$	Condition upstream of the blade
P	Particle
PS	Pressure side of the blade
SS	Suction side of the blade
T	Stagnation condition

INTRODUCTION
Present research work at the LTT focuses on the effects of flutter in turbomachinery. Under certain conditions, a blade row operating in a uniform flow field can enter into a self-excited oscillation known as flutter. The blade motion is sustained by the extraction of energy from the uniform flow during each vibratory cycle, with the flutter frequency corresponding generally to one of the lower blade or coupled blade-disk natural frequencies. The outstanding feature of flutter is that it leads to rapidly increasing blade vibrations which can destroy the engine Fleeter (1987).

Very often the aerodynamic phenomenon of flutter is simulated by means of artificially created forced vibration of the blades. In these vibration systems the mode, frequency and amplitude of vibration can easily be controlled, so that the flutter conditions can safely be simulated in an experiment.

The forced response problem encompasses potential flow interactions between fixed and rotating blade rows, as well as periodic impingement of upstream-generated wakes or shocks on downstream blading. These forced response phenomena remain a primary concern in gas turbine engine design and have important implications for engine life and reliability. In cases where the frequency of the aerodynamic forcing function matches the eigenfrequency of the blade structure, significant vibrations can occur and lead to structural fatigue and eventual failure.

To date, a significant research effort has been devoted to the quantification of the unsteady blade loading induced by such aerodynamic disturbances. Combined with knowledge of the structural characteristics of the blade assembly, this information can be used to predict blade vibration amplitudes and ultimately to determine the susceptibility of the blade to forced response phenomena. In order to avoid failure of the turbine components and to

To be Presented at the
15th Bi-annual Symposium on Measurement Techniques in Transonic and Supersonic Flow in Cascades and Turbomachines
University of Florence, 21-22 Sept. 2000

increase the efficiency of the turbomachine, a better understanding of the flutter phenomenon is required.

For the measurement of these unsteady flow fields, time-averaging measurement techniques are typically used. These techniques measure the unsteady flow fluctuations of pressure and velocity at single points on surfaces (pressure transducers, hot-film etc.) or single points in the flow field (LDA, L2F, hotwire probes etc.).

However, all these methods have in common that they cannot resolve the instantaneous features of the flow field, but can only provide field velocity data in statistical form.

One measurement technique that is able to provide instantaneous flow field data is the Particle Image Velocimetry (Adrian (1991), Liu et al (1991), Willert et al (1995)). The PIV technique yields good results for the investigation of transonic and supersonic flows (Bryanston-Cross (1995), Bryanston-Cross et al (1991), Höcker (1990), Kompenhans et al (1988), Towers et al (1991)). Previous published applications of the PIV method to turbine-like flow problems include external blade cooling (Langowski et al (1994)) or for "Dynamic Stall in a Pitching-Mode of a Wing" (Kompenhans et al (1994), Wernert (1995)). A good selection of PIV papers can be found in Grant (1994). Visser et al (1995) investigated the 3D flow field of a radial pump impeller. Grant et al (1994) and Tisserant et al (1995) applied the PIV method to the investigation of rotor-stator interaction in turbomachines.

The ability of PIV to measure the instantaneous flow field around the blade makes it an ideal technique to investigate blade vibration and forced response phenomena. To the knowledge of the authors this is the first application of the PIV method to this type of problem.

For the investigation of the blade vibration and forced response phenomena it seems to be promising to use the PIV measuring technique, since this technique can measure the instantaneous full flow field around the blade.

EXPERIMENTAL SETUP

Test Facility

The experimental measurements were conducted in the *Unsteady Transonic Wind Tunnel* (Figure 1) at the Ecole Polytechnique Fédérale de Lausanne. Air is supplied to this open cycle facility on a continuous basis by a four-stage centrifugal compressor with a pressure ratio of 3.5 and maximum flow rate of 10 kg/s. The air enters the tunnel through an inlet settling chamber and is accelerated by a converging nozzle into a rectangular test section measuring 200 mm (height) by 40 mm (width). The air exiting the test section is vented through a downstream valve to the atmosphere.

A single compressor blade with a NACA 3506 profile and a chord length of 78 mm is centrally mounted in the test section. The blade is made of Plexiglas to be traversed by the light sheet in order to avoid reflections in the test section. A vibration system driven by a hydraulic motor is externally attached to the blade.

The rotational motion of the motor is translated to a plunging blade vibration perpendicular to the chord via an eccentric shaft and connecting arm. The vibration frequency can be varied between 0 and 100 Hz, and the average amplitude is approximately 0.4 mm. The entire blade-motor assembly is mounted to the tunnel side-wall via a circular disc to allow easy adjustment of the inlet flow incidence angle. Within this disk, the blade entry passage is equipped with a specially designed labyrinth sealing system, which is described in further detail by Bölcs and Norryd (1994). This system significantly reduces the effects of flow leakage on the steady and unsteady measurements, while still ensuring an unrestricted motion of the blade.

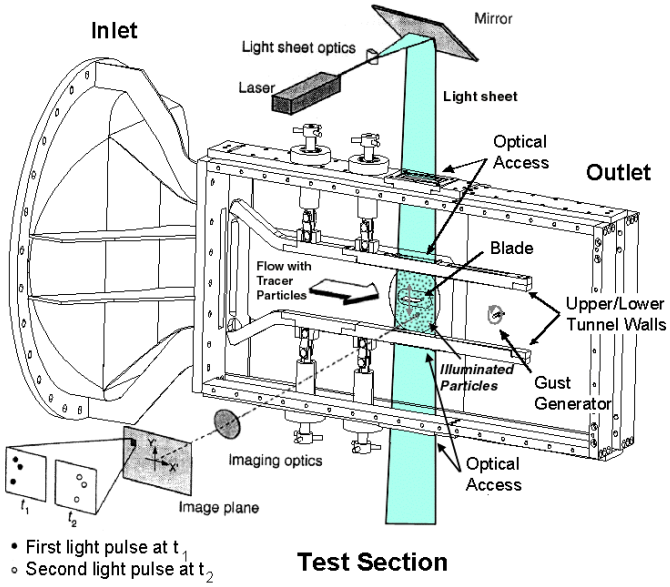

Figure 1: *The Unsteady Transonic Wind Tunnel*

Approximately 375 mm downstream of the blade mid-chord, a small flat plate (15 mm high, 39 mm wide and 2 mm thick) is mounted within the rotating shaft of a second hydraulic motor. The rotational frequency of this assembly can be varied between 0 and 100 Hz, producing upstream-running waves at twice the frequency (i.e. 0 to 200 Hz).

The above excitation systems, which are described in further detail by Lehr and Bölcs (2000), can be precisely synchronized and the phase lag between them can be freely varied. This allows for unsteady measurements to be conducted in the presence of only the downstream perturbation, only the blade vibration, or a combination of the two for different phase angles.

The PIV system

The laser used for the experiments is a Quantel TwinsB Nd-Yag high-energy double oscillator pulsed laser. The time delay between a pair of pulses can be adjusted from 1 μs to 1 s. The laser provides light pulses with a maximum energy of 320 mJ at a wavelength of 532 nm.

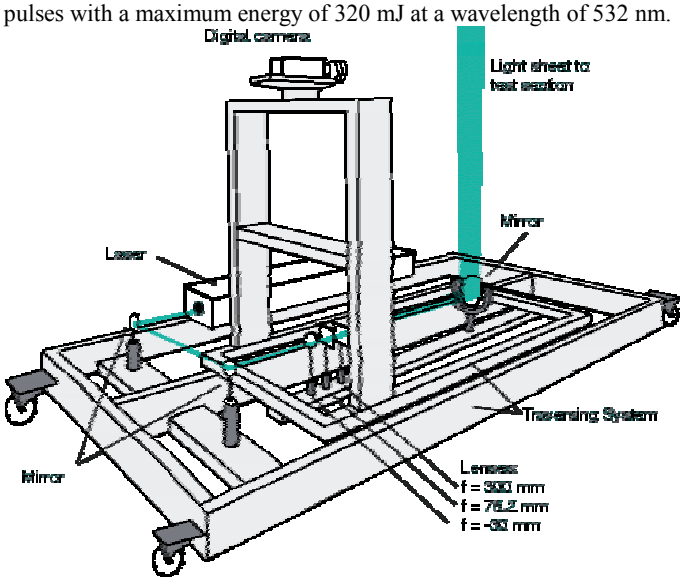

Figure 2: *Particle Image Velocimetry setup*

The pulse duration is approximately 5 ns with a peak power of 64 MW. A plano-concave lens (-30 mm focal length) combined with two plano-cylindrical lenses (76.2 and 300 mm focal length) transform the laser beam into a thin vertical light sheet. By adjusting the distance between these lenses, the desired thickness and width of the light sheet can be obtained. All lenses have an anti-reflecting coating.

The light scattered by the particles is recorded in a plane parallel to the light sheet. For the recording of the scattered light a Kodak ES 1.0 camera is used. This camera has a CCD interline transfer sensor, which has a pixels array of 1008 (H) by 1018 (V) pixels. Each pixel measures nine microns square with a 60% fill factor using a micro lens. The camera outputs 8 bit digital images with 256 gray levels. For PIV applications the camera is used in a special double exposure frame-triggering mode. This mode allows the capture of two images separated by a delay ranging from 2 µs to 66 ms. A Nikkor 55 mm micro lens is mounted on the camera. The F-number is adjusted to 2.8. For a typical recording situation, the distance between the camera and the light sheet is approximately 70 cm.

The complete system including laser, light sheet optics and camera is mounted on a traversing system that allows an easy displacement of the light sheet to the position of interest (Figure 2).

Data acquisition and processing

Since the out-of-plane component of the flow in the *Unsteady Transonic Wind Tunnel* (Figure 1) is two orders of magnitude smaller than the in-plane component, a single camera PIV system was used rather than a stereoscopic one.

Figure 3 shows the complete PIV data acquisition system that was assembled around the camera. The steady-state flow conditions are determined from the inlet plenum total pressure and temperature and static pressures measured along the test section side wall axially upstream the compressor blade. For steady-state flow field measurements by means of PIV the laser was triggered internally with a frequency of 10 Hz. The digital camera and the frame grabber are synchronized on the double laser pulses. The time separation between the two laser pules was set to 2.5 µs. For unsteady measurements the laser was triggered on a selected phase angle of the vibrating blade and the rotating flat plate of the gust generator, respectively, refer to Figure 4.

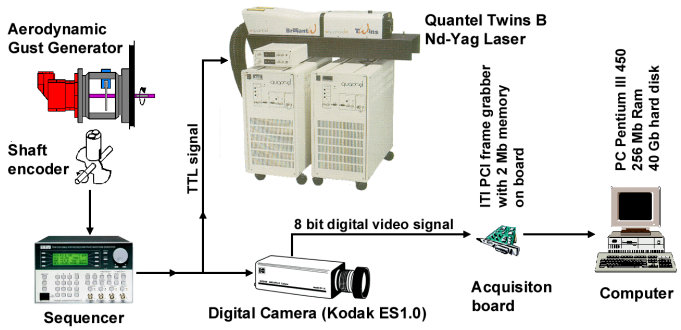

Figure 3: *Data acquisition system*

The PIV image acquisition starts with a TTL signal from the laser in a steady-state case and a TTL signal from the shaft encoder in an unsteady case, respectively. Two images are captured in rapid succession. This is accomplished by capturing the first image in the photo diode array, transferring this image to the CCD array and then capturing a second image in the photo diode array. The first image is transferred from the CCD array to the frame grabber while the second image is being captured by the photo diode array. The second image is then transferred into the CCD array and subsequently onto the frame grabber's second image buffer. The frame grabber is an Imaging Technology PCI frame grabber with 2 MB memory onboard. The PC is equipped with 256 MB RAM and 40 GB hard disk space. During the PIV measurement series, 50 image pairs are written in real time into the PC's RAM memory. Subsequently, the acquisition is stopped and the images are saved on the hard disk.

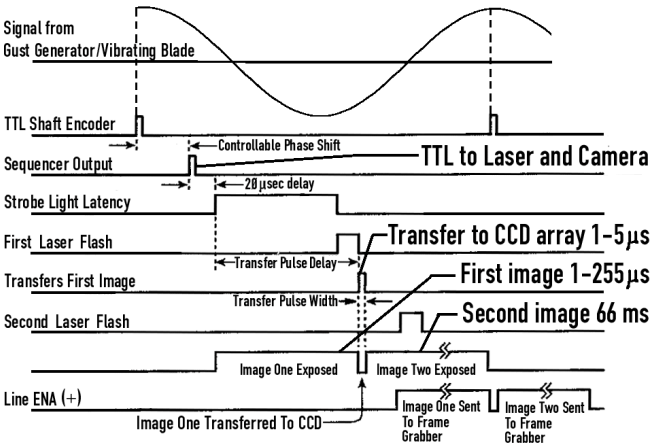

Figure 4: *Timing diagram for the image acquisition*

The PIV recordings from the camera are interrogated with the PIV software package VISIFLOW from AEA Technology. For the images, a cross-correlation analysis method is used with interrogation window sizes of 16 x 16 pixels and 32 x 32 pixels that correspond in the light-sheet to an area of approximately 0.5 x 0.5 mm^2 and 0.9 x 0.9 mm^2 respectively. The interrogation windows were overlapped by 50%. Since the camera acquires images with a resolution of 1008 by 1018 pixels, each recording results in a 120 by 120 vector field of instantaneous velocity.

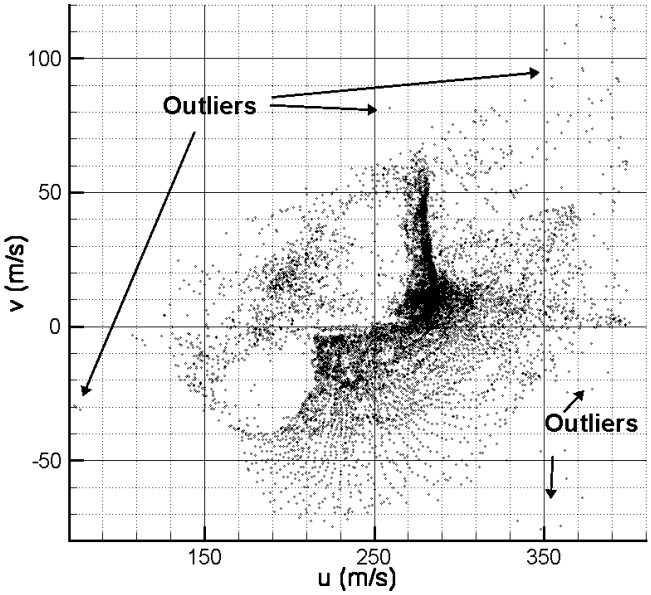

Figure 5: *Histogram of all vectors found by correlation in the whole flow field*

Due to the presence of reflections (blade, side-wall sealings, etc.) usually the data set contains a small number of spurious vectors (<5%). The vector field is therefore validated with predefined thresholds for the vector continuity and velocity magnitude. Vectors

that do not fall within the thresholds are removed and replaced by vectors with a lower correlation peak order. Due to the reflection problem a systematic error in the calculation of the vectors may occur. These vectors are detected and removed, too.

One suitable procedure to detect spurious data, especially in high speed flows with one dominating flow direction, is the global histogram of the raw data (Raffel et al (1998)) as shown in Figure 5. It is an equivalent representation of the vector map (Figure 10). Each point represents the velocity vector obtained by cross-correlation in a small interrogation window across the whole flow field. One can observe the main flow regions, a supersonic and a subsonic region. Furthermore, some outliers can be detected, that make physically no sense, e.g. upper and lower right corner in Figure 5. This method has been successfully used to remove spurious data in a first step.

In a second step most of the spurious vectors due to reflections are removed. This is realized by an in-house software, which automatically detects zones of reflections appearing in both frames used for the correlation and filters them out.

A weighted average of surrounding vectors fill the remaining gaps. The weighted average of surrounding vectors is calculated according to:

$$WeightedAverage = \frac{1}{N}\sum_{i=1}^{N}\left(v_i \cdot r^n\right)$$

with N: number of surrounding vectors taken into account
v_i: velocity of vector ***i***
r: fit radius, i.e. distance of the vector ***i*** from the center of averaging circle
n: fit power[1]

Tracer Particles

For most of the PIV measurements a Laskin nozzle generator has been used to produce the seeding particles, using the solvent DEHS (Di-Ethyl-Hexyl-Sebacat). DEHS is a non soluble, colorless and odorless liquid that evaporates completely after long time. A droplet with a 0.3 µm diameter has a life time of approximately 4 hours. Figure 6 shows the particle size distribution of DEHS particles for the same conditions as used for all experiments.

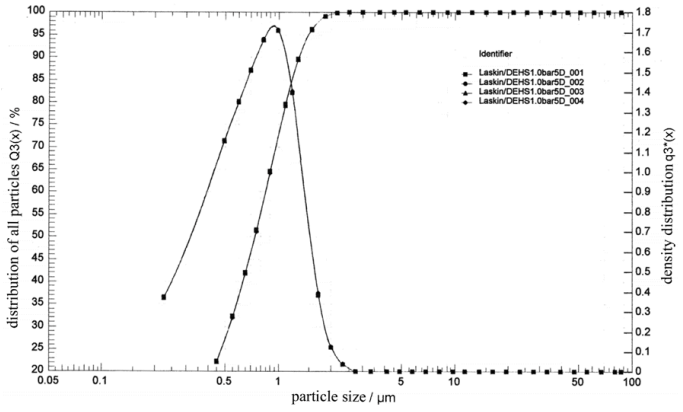

Figure 6: *Particle size distribution for DEHS*

For high speed PIV applications the generation of the particles is of the utmost importance (Melling (1997)). At a flow velocity of e.g. 300 m/s, the particle images have moved approximately 1.6 µm in the recording plane during the length of a single laser pulse (5 ns). This distance is much smaller than the diameter of the particle images. Thus, blurring of the particle images is avoided by the very short duration of the laser pulse. At the same flow velocity a time delay between the two laser pulses of 2.5 µs was used to obtain a sufficient displacement of approximately 240 µm (≈12 pixels) between the two particle images in the recording plane. The density of particle images in the recording plane was high enough to find images of several particle pairs within the interrogation windows in most cases.

A primary source of error is the influence of gravitational forces, if the density of the fluid ρ and the tracer particles ρ_P do not match. Especially in flows with strong velocity gradients, e.g. shocks, this effect has to be taken into account. Therefore the step response of the particle velocity U_p has been investigated by Raffel et al (1998). U_p typically follows an exponential law, if the density of the particle is much greater than the fluid density:

$$U_p(t) = \left[1 - \exp\left(-\frac{t}{\tau_s}\right)\right]$$

The result of this equation is illustrated in Figure 7 where the time response of DEHS particles with different diameters is shown for a strong deceleration, i.e. a normal shock in an air flow.

Since the size of the DEHS particles used in this paper is slightly smaller than 1 micron, the particles have reached 90% of the speed after the shock already after less then 5 µs. This yields a rounded Mach number distribution over the shock and a slightly smeared shock position, Figure 12. However, since ensemble-averaging of the pictures has the same effect, the above behaviour of the particles is good enough to predict both shock strength and shock position accuratly within the limits of the assembled measurement system.

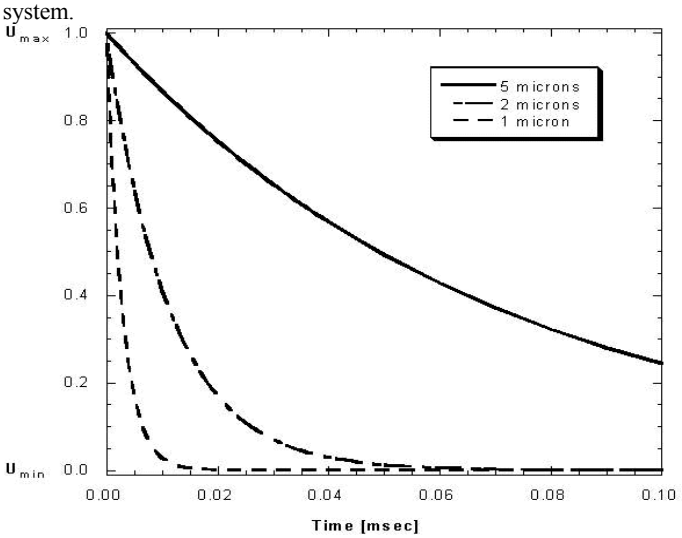

Figure 7: *Time response of DEHS particles with different diameters in a decelerating flow*

When the particles and thus the particle images become too small a specific effect can be observed in the observed data: the displacements tend to be biased towards integral values (Figure 8). The effect increases as the particle image diameter is reduced. This effect is well known in literature and is referred to as "peak-locking" or as "bias error" (Raffel et al (1998), Melling (1997)).

A variety of solutions exist to remove this effect. First the particle image diameter can be increased. This can be realized even by

[1] Higher (more negative) values of ***n*** give more importance to vectors near the center of the circle. Setting ***n*** to zero gives equal weighting to all vectors in the fitting circle. Recommended: ***n*** = **-2**

slightly defocusing the particle image This has been done for some results shown in this paper. However, choosing a different peak estimator that is better suited for smaller particle image diameters is the best choice. For all results shown in this paper a three-point Gaussian peak fit estimator was used, for which no peak-locking effect occurred.

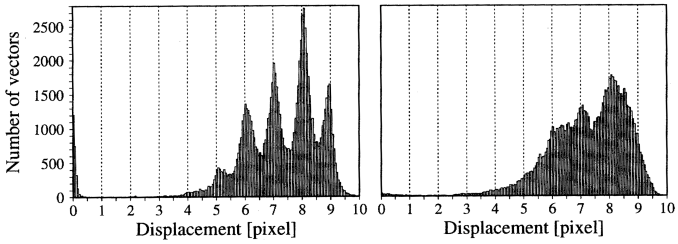

Figure 8: *Histogram of PIV displacements with "peak-locking" (left) and with removed effect (right) [Raffel et al (1998)]*

MEASUREMENTS PROGRAM AND FLOW CONDITION

For all results shown in the present work the Reynolds number based on the chord length and the inlet velocity was $Re=1.18 \times 10^6$. The inlet Mach number was fixed to $M_\infty = 0.6$ or $M_\infty = 65$. The inlet total temperature was set to $T_T = 305$ K. These values were evaluated from static pressure measurements at the entrance of the test section, approximately two chord lengths upstream the leading edge of the blade, and total pressure and temperature measurements in the settling chamber.

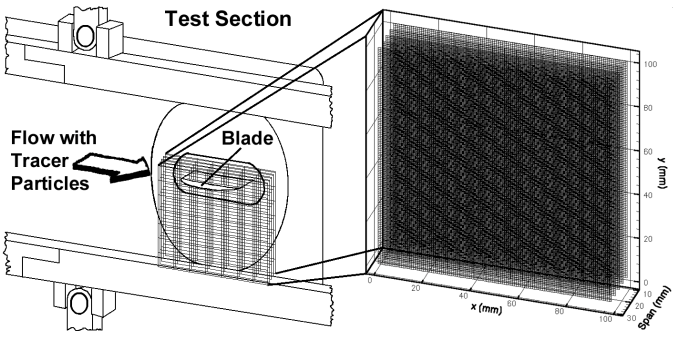

Figure 9: *Nine measurement planes in the test section (between 25% and 75% of span in steps of 6.25%)*

Testing was conducted for a single flow incidence angle of $i = 5°$. Unsteady tests were performed with a fixed blade and pressure perturbations created by the gust generator at frequencies between 20 Hz and 50 Hz (k=0.0225 and 0.0562) in steps of 10 Hz. For unsteady tests the measurement system was triggered on eight phase angles $0° < \varphi < 360°$ that corresponds to one excitation cycle (i.e. half a rotation of the flat plate) of the gust generator. For steady-state measurements the position of the flat plate was fixed at an angle of $\cos \varphi = 0.5$, i.e. the average blockage of the rotating plate.

Due to reflections in the test section measurements could not be conducted close to the side walls. Thus, the flow field was measured in nine planes between 25% and 75% of the span in steps of 6.25%, this corresponds to sections between 10 mm and 30 mm of blade height in steps of 2.5 mm. The situation of the measurement planes is shown in Figure 9.

UNCERTAINTY

For the estimation of the uncertainty of PIV velocity measurements many parameters have to be considered (Raffel et al (1998)). Systematic errors occur due to the uncertainty in the determination of the geometrical parameters and the fabrication tolerances of the camera devices and lenses. Non-systematic errors are mainly due to the uncertainty in the determination of the average particle displacement in the interrogation region. These depend on the size of the interrogation region, the time separation between the laser pulses, the magnification of the recording, the out-of-plane velocity component, the turbulence and the length scale of the flow etc. The choice of the recording and interrogation parameters is therefore of significant importance for accurate and reliable velocity measurements. As the flow in the test section is quasi two-dimensional, the out of plane component of the vectors causes only negligible errors.

To quantify the uncertainty of the presented PIV measurements an experimental study has been conducted by Schabacker et al (1996). Typically 50 field samples were ensemble averaged on each measurement plane and for each phase angle. From these measurements it was determined that the 95% confidence interval for the mean velocity field is less than 0.08 U_∞, in regions of strong velocity gradients it is smaller than 0.1 U_∞. Whereas the determination of the position of the shock depends mainly on the maximum size of the interrogation window. Therefore, the position of the shock for instantaneous data sets can be determined with an error in the order of 0.5% of the chord length of the blade.

RESULTS AND DISCUSSION OF THE FLOW

Steady-state results

In this section some steady-state results will be presented. They will be depicted in two different forms: the ensemble average of 50 individual instantaneous data sets, and the instantaneous flow fields themselves. Although the uncertainty level for the imstantaneous results is about twice that for the ensemble-averaged ones, they provide a good insight into the time-dependent behaviour of the so-called steady-state flow condition.

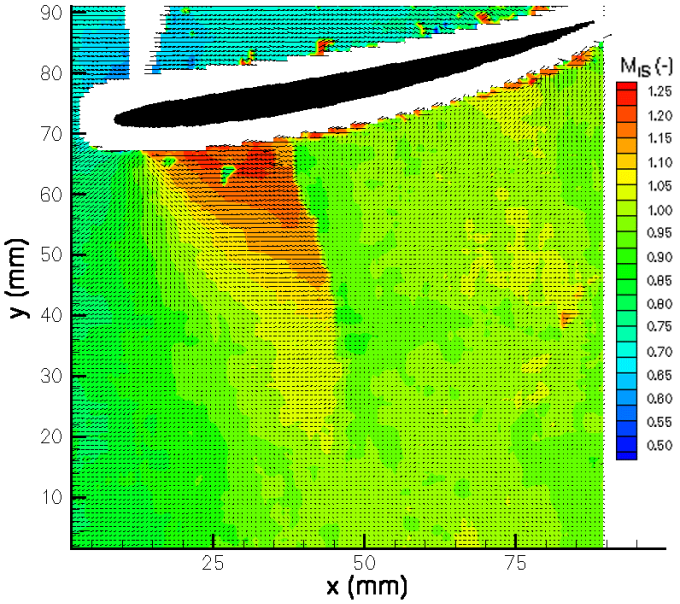

Figure 10: *Instantaneous velocity disturbances $V\text{-}V_{mean}$ and isentropic Mach number field, M_∞ =0.65, steady-state case, mid-span plane*

A typical example of the instantaneous velocity-vector map is shown in Figure 10. The Mach number magnitude is colour-coded.

The normal shock on the suction side of the blade is situated at 35% of the chord length. Although approximately 2.5% of all vectors were automatically detected as spurious by the in house software, there still remain some obviously false vectors especially close to the blade. These occur due to reflection problems in the proximity of the blade and have to be manually removed. Another region in the flow field,

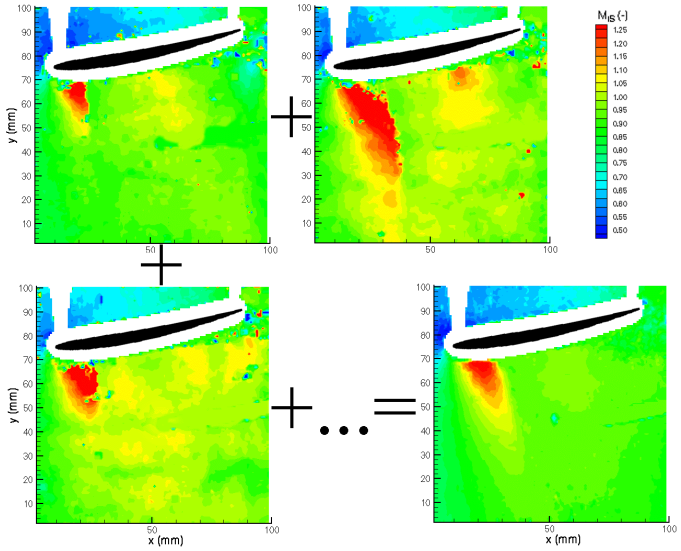

Figure 11: *Instantaneous (upper and lower left) and ensemble-averaged (lower right) isentropic Mach number field of the steady state flow field, M_∞ =0.65, mid-span plane*

where no valid correlation can be obtained is above the blade at the leading edge (Figure 10) and trailing edge (Figure 11). This is due to the curvature of the leading edge and trailing edge of the blade that refracts the laser light arriving from the bottom causing a shadowed zone on the upper side. In these regions no particles are illuminated and therefore no correlation can be found.

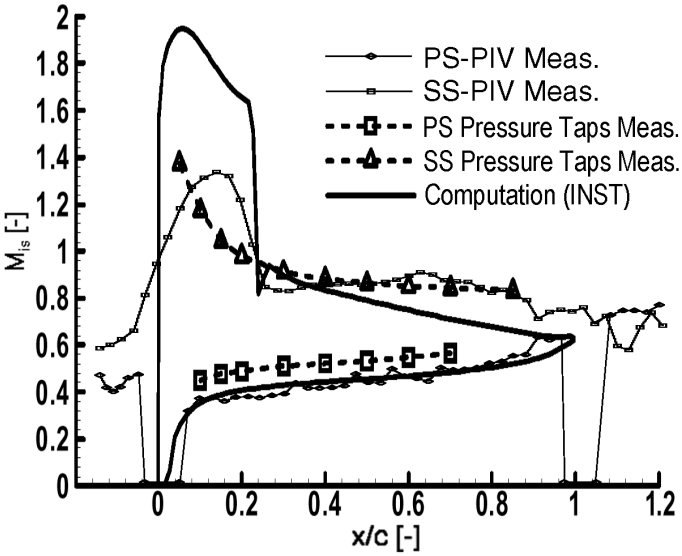

Figure 12: *Isentropic Mach number distribution on streamlines close to the blade surface (approx. 5 mm for PIV-measurements), on the blade surface for pressure taps measurements and calculation, M_∞ =0.60, i = 5° (refer to Nowinski (1999))*

In particular, Figure 10 shows the final grid spacing obtained for all experiments that correspond to a spatial resolution in the flow field of approximately 0.5 mm.

To obtain the averaged flow field for the steady-state flow condition the instantaneous data sets are ensemble-averaged. Three examples of the instantaneous (upper and lower left) and the ensemble-averaged flow field (lower right) are depicted in Figure 11. The supersonic region in each picture is followed by a strong normal shock.

Despite the steady-state flow condition the size of the supersonic region can vary drastically. These fluctuations are caused by the pressure variations induced by the unsteady wake flow. The shock position in the instantaneous pictures is approximately fixed. It varies only about 2% of chord. This explains the slightly smeared shock position in the ensemble-averaged picture (Figure 11, lower right). Nevertheless, the determination of the shock position in the ensemble-averaged flow field is still very good and in the order of magnitude of the resolution of the PIV measurement technique.

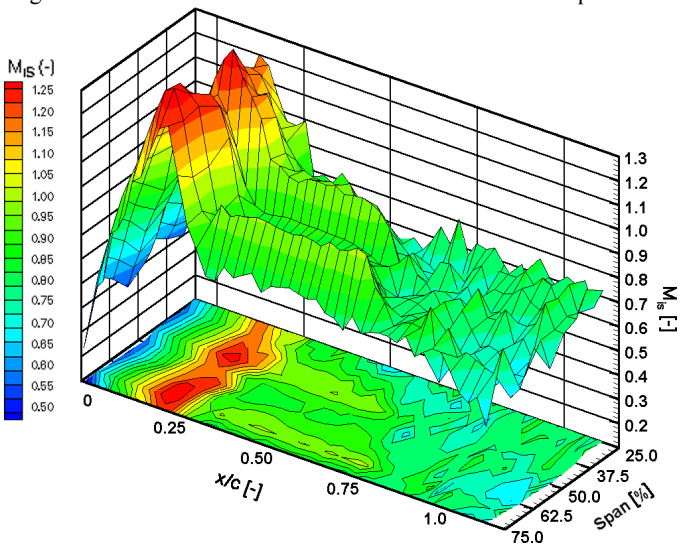

Figure 13: *Isentropic Mach number distribution close to the blade surface (approximately 5 mm), M_∞ =0.65, i = 5°*

To validate the PIV method the steady-state results have been compared to pressure taps measurements on the blade surface (Nowinski (1999)) and to calculations with the INST code developed by Ott (1992), refer to Figure 12. The INST code is based on the conservative form of the two-dimensional, time-dependent Euler equations.

The PIV data set for Figure 12 has been extracted from streamlines near (approximately 5 mm) to the blade surface. On the suction side there is a strong acceleration up to about 25% of chord followed by a strong normal shock. Due to boundary layer effects in the pressure taps measurements, the shock location on the suction side of the blade is completely smeared. The PIV measurements are in good agreement with the pressure taps measurements but reveal the supersonic flow region. However, the position of the shock is smeared, too. This effect is due to the ensemble-averaging of the individual data sets. The isentropic Mach number distribution of the PIV measurements also highlights the gap of values on the pressure side above the leading and trailing edge of the blade due to the shadowed zones in the flow field (Figure 12).

The theoretical results obtained with the INST code show the same location of the normal shock on the blade (approximately 25% of chord). However, the supersonic acceleration is strongly overestimated. On the other hand, due to the absence of the side wall boundary layers in the INST code the calculated flow does not feel the same acceleration as in the measurements. Therefore the Mach

number level at the trailing edge of the blade tends to be underestimated.

To quantify the steady state flow field in the test section, measurements were conducted on nine planes in span-wise direction. The location of the normal shock over the whole span is approximately at 22% of chord (refer to Figure 13). Close to the hub wall (25-30% of span) the supersonic flow region becomes smaller. This is due to the leakage flow caused by the labyrinth sealing of the blade support. This leakage flow influences the main flow up to 50% of span. A developed two-dimensional flow field can only be observed between 50% and 75% of span. However, at 75% of span the boundary layer of the outer side wall and the tip leakage flow is already noticeable.

Pressure sensitive paint (PSP) measurements using the same geometry and flow condition as in Figure 13 have been recently conducted in the same test facility (not presented in this paper). Although PSP measurements are taken on the blade surface itself, the evaluation of these results yields similar behaviour of the flow field in the test section.

Phase-averaged results with gust generator perturbation

The objective of these tests is to investigate the time dependence of the flow field in the presence of a downstream created pressure variation. To obtain the illustrations shown in this section, for each phase – frequency case 50 individual instantaneous data sets are ensemble averaged.

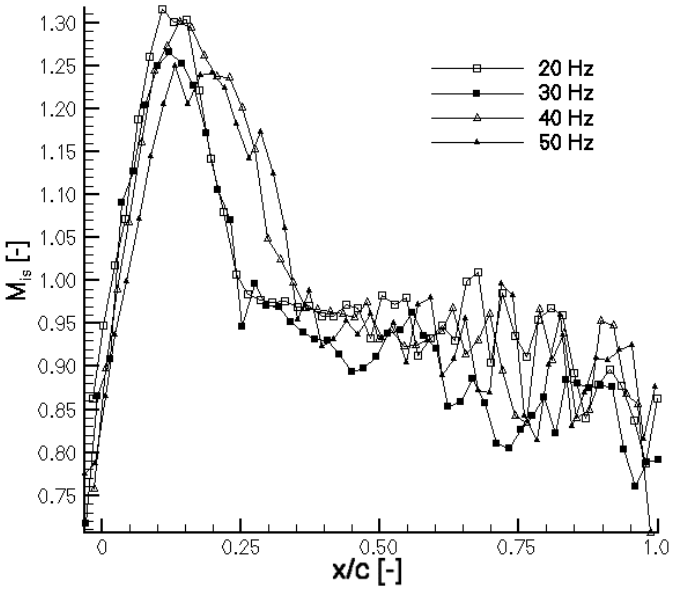

Figure 14: *Isentropic Mach number distribution for different frequencies of the rotating blade (gust generator), mid-span, M_∞ =0.65, i = 5°, phase angle $\varphi = 135°$*

The phase-averaged results of the unsteady measurements for four different excitation frequencies of 20 Hz to 50 Hz (k=0.0225 and 0.0562) in steps of 10 Hz are shown in Figure 14. The isentropic Mach number distribution is quite similar for the 20 Hz and 30 Hz cases, the shock position is situated at approximately 20% of chord. For increased frequencies, 40 Hz and 50 Hz, the location of the shock tends to move downstream to 30% and 33% of chord, respectively.

For higher frequencies the time scale of the vibration decreases and therefore reduces the section in which the shock position can fluctuate. Hence, the location of the shock moves downstream for increasing frequencies until attaining a frequency at which the flow and the supersonic region with the terminating shock no longer change in time. In some single individual frames flow separation occurs. This effect may introduce an additional noise in the phase-averaged data set. This phenomenon is most important for the phase angle of $\varphi = 135°$ shown in Figure 14 and starts at approximately 60% of chord. To avoid the introduction of this additional error the sample number must be significantly increased. In Figure 15 this phenomenon does not occur that drastically due to a careful pre-selection of the data sets taken into account for the phase averaging.

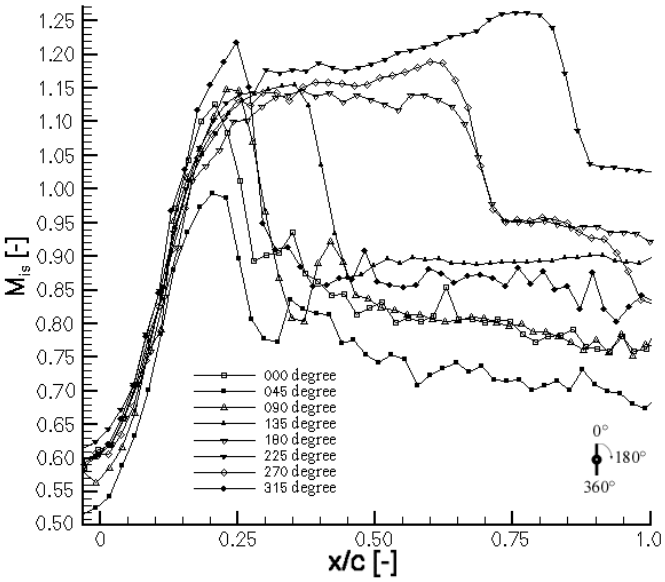

Figure 15: *Isentropic Mach number distribution on the suction side with a rotating plate (gust generator) at different phase angles, mid-span, M_∞ =0.65, i = 5°, f=20 Hz*

Figure 15 represents the isentropic Mach number distribution for one complete cycle of the gust generator in steps of $\Delta\varphi = 45°$ for the phase angle at an excitation frequency of f = 20 Hz. At a vertical position of the flat plate ($\varphi = 0°$) the exit of the test section is blocked about 20% of the height. Due to this blockage significant flow deceleration occurs. However, the lowest Mach number is obtained for a phase angle of $\varphi = 45°$, the flow experiences the highest acceleration for $\varphi = 270°$. Thus, there exists a phase shift of approximately $\Phi = 45°$ between the excitation source and the aerodynamic response of the flow. In these results the resolution of discrete angles at which PIV measurements are conducted is not high enough to determine more precisely the phase angle Φ.

The region in that supersonic flow occurs changes considerably. The location of the strong normal shock terminating this region varies between 25% of chord for $\varphi = 45°$ and 85% for a phase angle of $\varphi = 270°$. This implies harsh changes in the aerodynamic loading of the blade (refer to Figure 15).

The phase averaged flow field information for different positions of the flat plate (gust generator) at a frequency of f = 20 Hz is shown in Figure 16 at the border, the steady state ensemble averaged flow field for the same flow conditions (M_∞ =0.65, i = 5°) in the centre. Those snapshots of the flow field at several time instants over one excitation cycle show the important fluctuations of the flow over the whole test section. For phase angles $135° < \varphi < 270°$ the supersonic flow region almost reaches down to the lower wall of the test section.

SUMMARY AND CONCLUSIONS

An existing Particle Image Velocimetry measurement system has been adapted to the requirements of the newly introduced *Unsteady Transonic Wind Tunnel* (Nowinski (1999)). With this PIV measurement technique it is possible to gather instantaneous flow field information across planes in the test section both, under steady state conditions and in the presence of oscillating perturbations. The objective of these tests was to provide some fundamental knowledge on the instantaneous flow behaviour of the steady state flow, and the unsteady flow field in the presence of downstream created pressure perturbations introduced by a gust generator. Unsteady tests were conducted at reduced frequencies between 0.02 and 0.06 in nine different planes between 25% and 75% of span. From this work, the primary observations and conclusions are as follows:

- The Particle Image Velocimetry (PIV) technique has been applied to the flow conditions of the *Unsteady Transonic Wind Tunnel* and its performance was validated with pressure taps measurements and calculations.
- The PIV measurement technique is suited to reveal the flow fluctuations that occur even for steady-state experiments in transonic flow conditions, especially the size and location of the supersonic flow region and shock position.
- Due to the flow leakage from the labyrinth sealing system used in the *Unsteady Transonic Wind Tunnel*, the region in which the flow can be considered as two-dimensional is not at the centre of the test section. It is located between 50% and 75% of span.
- The flow field sustains strong variations in the presence of downstream created pressure perturbations introduced by a gust generator. Those tend to become less important for higher frequencies. To confirm this tendency detailed investigation of the flow at higher frequencies must be conducted.

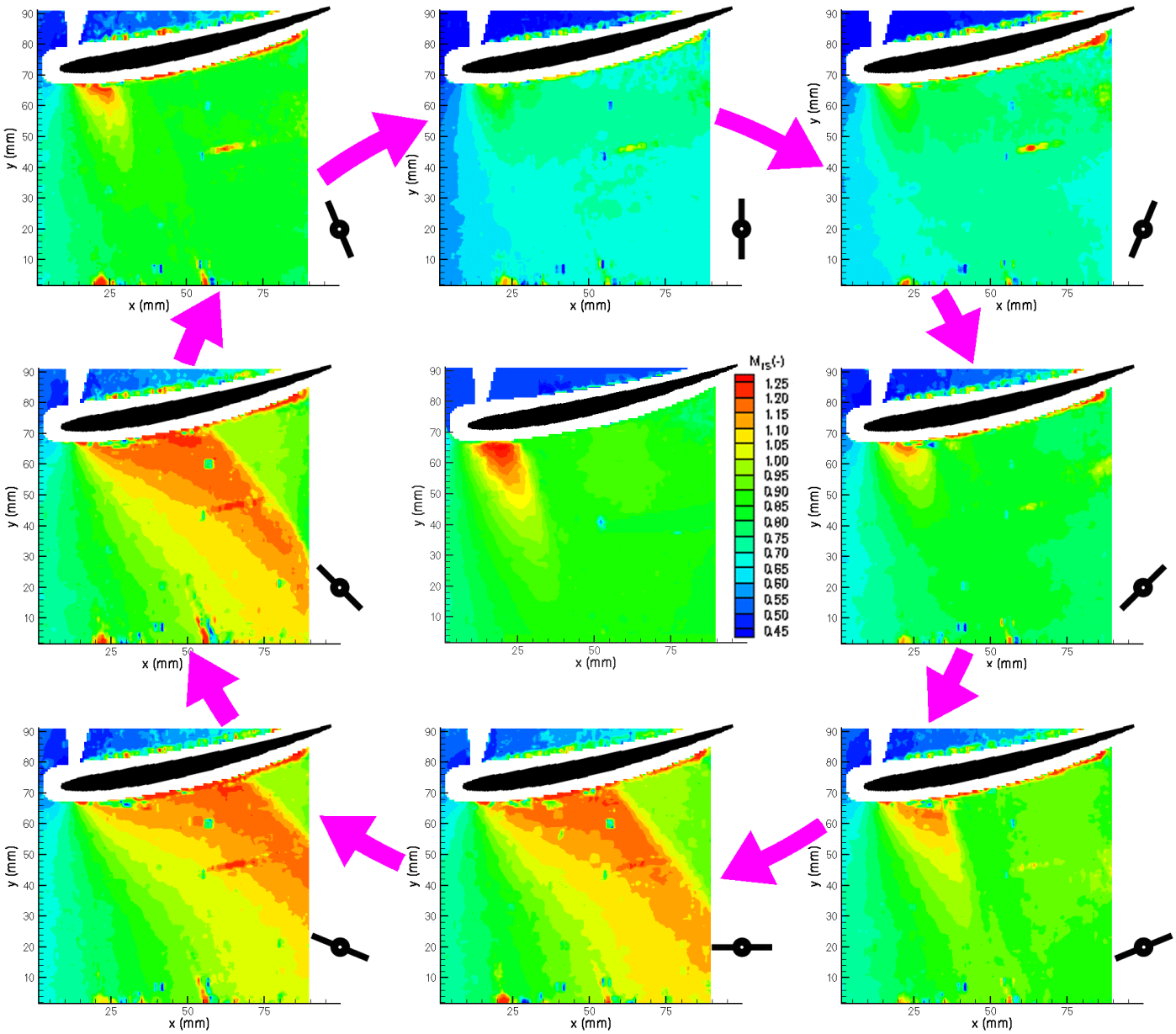

Figure 16: *Time-variant flow field (phase-averaged, 50 samples) for different positions of the rotating flat plate (gust generator) f = 20 Hz,. steady state flow field in the centre, M_∞ =0.65, mid-span position*

- The unsteady measurements reveal a phase angle Φ between excitation source and the aerodynamic response. However, the PIV method only takes snapshots of the flow field at discrete instants of the excitation cycle. Hence, more discrete phase angles have to be taken into account in order to determinate more precisely the phase angle Φ .

FUTURE WORK

The results presented in this paper represent only preliminary measurements. Continuing work will concentrate on investigating the flow field in the test section around the vibrating blade in a sinusoidal plunging mode. A controlled combination of the blade vibration and the downstream created gusts will complete the series of experiments to validate the superposition principle for forced response (superposition principle: unsteady loading resulting from the combined excitation of the blade can be accurately predicted by a linear superposition of the individual gust and blade vibration-induced flow fields). A wider range of reduced frequencies and a better resolution of phase angles will therefore be covered.

In addition, measurements with fast-response aerodynamic probes (FRAP®) are planned to validate the two measurement techniques using different physical principles and enhance the experience with FRAP® probes in unsteady transonic flows. These measurements are conducted in collaboration with the Swiss Federal Institute of Technology, LSM-ETH, at Zurich, Switzerland.

ACKNOWLEDGEMENTS

This work is supported by the Ecole Polytechnique Fédérale de Lausanne and the Leonhard Euler Centre, Swiss ERCOFTAC Pilot Centre. The authors wish to express their appreciation for permission to publish these results.

REFERENCES

Adrian R.J.; 1991: Particle-Imaging Techniques for Experimental Fluid Mechanics, *Annual. Rev. Fluid Mech., no.23, pp. 261-304*

Bölcs A., Norryd M., 1994: Development of a Sealing Construction to Prevent Leakage Flow During Flutter Tests in a Linear Cascade, *12th Symposium on Measuring Techniques for Transonic and Supersonic Flow in Cascades and Turbomachines, Prague, 12-13 Sept. 1994*

Bryanston-Cross P.J.; 1995: The Application of PIV (Particle Image Velocimetry) to Transonic Flow Measurements, *CH34827-95/0000-53.1, IEEE 1995*

Bryanston-Cross, Towers P.J., Judges C.E., Harasgama D.P.; 1991: The application of particle image velocimetry in a short duration transonic annular turbine cascade, *ASME paper 91-GT-221*

Fleeter S., Jay R.L.; 1987: Unsteady Aerodynamic Measurements in Flutter Research, *AGARD Manual on Aeroelasticity in Axial-Flow Turbomachines, AGARD-AG-298, Volume 1, 1987*

Grant I. (editor); 1994: Selected papers on Particle Image Velocimetry, *SPIE Milestone Series, Vol. MS 99*

Grant I., Pan X., Wang X., Stewart N.; 1994: Correction for Viewing Angle Applied to PIV Data Obtained in Aerodynamic Blade Vortex Interaction Studies, *Experiments in Fluids 18, pp. 95-99, Springer-Verlag 1994*

Höcker R.; 1990: Untersuchung der transsonischen Umströmung eines stumpfen Zylinders mit Hilfe der Geschwindigkeits-feldmeßmethode, *Dissertation, Georg-August-Universität zu Göttingen 1990*

Kompenhans J., Höcker R.; 1988: Application of Particle Image Velocimetry to High Speed Flows, *Particle Image Displacement Velocimetry, pp. 67-84, 1988 von Karman Institute for Fluid Dynamics*

Kompenhans J., Raffel M., Wernert P., Schäfer H.J.; 1994: Instantaneous Flow Field Measurements on Pitching Airfoils by Means of Particle Image Velocimetry, *Optical Methods and Data Processing in Heat and Fluid Flow, London, 14-15 April 1994*

Langowski C., Voigt P.; 1994: Film Cooling of an Annular Turbine Stator Visualisation of Cooling Air Ejection and its Effect on the Aerodynamic Losses, *12th Symposium on Measuring Techniques for Transonic and Supersonic Flow in Cascades and Turbomachines, Paper 19, Prague, Czech. Rep., September 12-13 1994*

Lehr A., Bölcs A., 2000: Application of a Particle Image Velocimetry System to the Investigation of Unsteady Transonic Flows in Turbomachinery, *9th International Symposium on Unsteady Aerodynamics, Aeroacoustics and Aeroelasticity of Turbomachines, Lyon, Sept. 4-8, 2000*

Liu Z.-C., Landreth C.C., Adrian R.J., Hanratty T.J.; 1991: High Resolution Measurement of Turbulent Structure in a Channel with Particle Image Velocimetry, *Experiments in Fluids 10, pp. 301-312*

Melling A., 1997: Tracer Particles and Seeding for Particle Image Velocimetry, *Measurement Science and Technology, Vol.8, No.12, pp. 1406-1416*

Nowinski, M., 1999: Experimental Investigation of an Oscillating Airfoil in the Presence of Downstream-Generated Aerodynamic Gusts, *Thèse No. 2072 (1999), EPFL, Lausanne*

Ott, P., 1992: Oszillierender senkrechter Verdichtungsstoß in einer ebenen Düse, *Communication du Laboratoire de Thermique Appliquée et de Turbomachines de l'Ecole Polytechnique Fédérale de Lausanne, No.18*

Raffel M., Willert C., Kompenhans J., 1998: Particle Image Velocimetry, A Practical Guide, *ISBN 3-540–63683-8, Springer-Verlag 1998*

Schabacker J., Bölcs A.; 1996: Investigation of Turbulent Flow by Means of the PIV Method, *Paper presented at the 13th Symposium on Measuring Techniques for Transonic and Supersonic Flows in Cascades and Turbomachines, Zurich, Switzerland, September 5-6 1996*

Tisserant D., Breugelmans F.A.E.; 1995: Rotor Blade – to - Blade Measurements using Particle Image Velocimetry, *ASME, 95-GT-99*

Towers C.E., Bryanston-Cross P.J., Judge T.R.;1991: Application of Particle Image Velocimetry to Large-Scale Transonic Wind Tunnels, *Optics & Laser Technology, Vol.23, No.5, 1991, pp. 289-295*

Visser F.C., Jonker J.B.;1995: Investigation of the Relative Flow in Low Specific Speed Model Centrifugal Pump Impellers Using Sweep-Beam PIV, *Flow Visualization VII, ISBN 1-56700-0363, 1995*

Wernert P., Koerber G., Wietrich F., Raffel M., Kompenhans J.; 1995: PIV Measurements and Laser-Sheet Visualization of the Unsteady Flowfield over an Airfoil Pitching in Dynamic Stall Conditions, *Flow Visualization VII, ISBN 1-56700-0363, 1995*

Willert C., Stasicki B., Raffel M., Kompenhans J.; 1995: A Digital Video Camera for Application of Particle Image Velocimetry in High-Speed Flows, *SPIE Proceedings Article No. 2546-19*